Thermal performance of a Cu-water nanofluid in a plate heat exchanger with a wavy wall in the presence of a magnetic field

Walid Nessab, Khaled Mouaici, Brahim Fersadou, Henda Kahalerras*

University of Sciences and Technology Houari Boumediene USTHB, Laboratory of Multiphase Transport and Porous Media LTPMP, BP 32 El Alia 16111 Bab Ezzouar, Algiers-Algeria, email: hkahalerras@usthb.dz (H. Kahalerras)

ABSTRACT

The performance of a plate heat exchanger with a thin wavy inner wall under a variable magnetic field, produced by six sources on each side of the outer plates, was investigated numerically. The hot and cold Cu-water nanofluids flowed co-currently and in forced convection mode in the lower and upper compartments. The finite volume approach and the SIMPLE algorithm were used to solve the governing equations and associated boundary conditions. The parametric study was focused on the Hartmann number, intensity ratio, and undulation amplitude effects. The results revealed that raising these parameters improved the heat exchanger effectiveness and the thermal performance coefficients η_{Ha} compared to the case without magnetic field, and η_{RI} compared to the situation with unitary intensity ratio. The largest values of η_{Ha} and η_{RI} were 28% and 17%, respectively.

Keywords: Nanofluid; Heat exchanger; Wavy wall; Magnetic field

1. Introduction

Heat exchangers are widely used in thermal systems for various industrial purposes. Heat transfer intensification in these thermal devices can be achieved using passive, active, or combined approaches. The use of nanofluids as working fluids for heat exchangers has evolved recently. A corrugated plate heat exchanger in a solar energy system was used by Zheng et al. [1] to examine the heat exchange and flow features of various nanofluids (Al_2O_3-30 nm, SiC-40 nm, CuO-30 nm, and Fe_3O_4-25 nm). A study's objective by Karuppasamy et al. [2] was to improve the heat transfer in a shell-and-tube heat exchanger by simultaneously employing nanofluids and cone-shaped inserts to create flow disturbances without significantly increasing the pumping power. The influence of various nanoparticles shapes on the thermal-hydraulic efficiency of a nanofluid flowing in a shell-and-tube heat exchanger was analyzed by Biheraei et al. [3]. The shell side was equipped with a novel form of inclined and trapezoidal baffles to develop a vortex flow. The performance of an (MWCNT-Fe_3O_4/water) hybrid nanofluid as a coolant in a plate heat exchanger was experimentally examined by Alklaibi et al. [4]. It was found that the exergy efficiency of a hybrid nanofluid was 10.5% higher than that of pure water.

Based on simple passive technologies for heat transfer enhancement, researchers have adopted new techniques combining active and passive processes. Biharaei and Hangi [5] investigated the efficiency of a magnetic nanofluid as a cooling fluid in a tubular heat exchanger exposed to an external magnetic field. The hot liquid was pure water and flowed counter-currently in the annular space. The magnetic field application led to a more uniform distribution of the nanoparticles. Mousavi et al. [6] examined the influence of a variable magnetic field on heat transfer occurring in a tubular heat exchanger with a sinusoidal inner tube. From a numerical study on the thermal-hydraulic behavior of a ferrofluid in a concentric tube heat exchanger, Shakiba

---

* Corresponding author.

and Vahedi [7] have deduced that applying a non-uniform transverse magnetic field might control the motion of the ferrofluid and thus improve the heat transfer. The simultaneous effects of several techniques for heat transfer enhancement (i.e., two passives: nanofluid and helical rib and two actives: pulsed flow and magnetic field) on the flow and heat transfer characteristics in a helically corrugated tube were experimentally analyzed by Naphon and Wiriyasart [8]. A test bench was performed by Mei et al. [9] to assess how well a water-Fe$_3$O$_4$ nanofluid performed thermo-hydraulically in a wavy tube while subjected to different magnetic fields. Wang et al. [10] experimentally investigated corrugated tubes' friction coefficient and heat exchange rate for varied pitches of corrugation. (TiO$_2$-H$_2$O) nanofluid and water were employed as heat transfer media. Fan et al. [11] conducted an experimental investigation in a heat exchanger using a corrugated tube, a perforated turbulator, a Fe$_3$O$_4$-water-arabic gum nanofluid as working fluid, and a controlled magnetic field to reduce the size of the device and save energy. According to the numerical investigation of Cao et al. [12], applying a magnetic field has extended the nanoparticles' transport region as they moved from hot to cold zones.

The present study aimed to improve the thermal performance of a plate heat exchanger using a technology combining three techniques: (Cu-water) nanofluid, sinusoidally wavy wall, and non-uniform magnetic field.

2. Mathematical formulation

2.1. Physical domain

The physical domain, illustrated in Fig. 1, was a plate heat exchanger composed of two compartments each of length l, mean height $H/2$ and separated by a thin wavy plate of amplitude a', undulations number n, and negligible thermal resistance. The working fluid was a water-copper nanofluid with a volume fraction of nanoparticles ϕ. The hot and cold liquids of the same nature, flowing co-currently in the lower and the upper compartment, respectively, entered the heat exchanger with uniform temperatures T_{hi} and T_{ci} and constant velocities U_{hi} and U_{ci}, respectively. A non-uniform magnetic field was created by six sources located outside the heat exchanger and staggeringly positioned in the vicinity of the upper (03 sources) and lower (03 sources) plates which were thermally insulated. Each magnetic source was an electric wire traversed by an
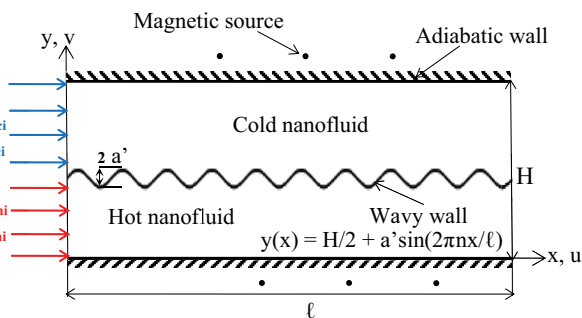
electric current I generating a magnetic induction B whose axial and transverse components were Eqs. (1a) and (1b):

$$B_x(x,y) = -\mu_o \frac{I_{l,\text{up}}}{2\pi} \frac{(y-b)}{(x-a)^2 + (y-b)^2} \tag{1a}$$

$$B_y(x,y) = +\mu_o \frac{I_{l,\text{up}}}{2\pi} \frac{(x-a)}{(x-a)^2 + (y-b)^2} \tag{1b}$$

Each source was recognized by its axial and transverse locations, denoted as a and b, respectively. I_l and I_{up} were the electric currents crossing the lower and upper sources.

2.2. Governing equations

The nanofluid was considered Newtonian, incompressible, and electrically conductive. The flow was steady-state, laminar, and two-dimensional. The thermophysical properties, considered constant, were the same for the hot and the cold fluids. Viscous dissipation was neglected, and there was no internal heat source. Local thermal equilibrium existed between the solid nanoparticles and the base fluid.

The continuity, momentum, and energy equations in forced convection mode were made dimensionless utilizing the reduced variables:

$$(X,Y) = \frac{(x,y)}{H}; \quad P = \frac{p}{\rho_{nf}U_{ci}^2}; \quad (U,V) = \frac{(u,v)}{U_{ci}};$$

$$(\bar{B}_X, \bar{B}_Y) = \frac{(\bar{B}_x, \bar{B}_y)}{B_0}; \quad B_0 = \mu_o \frac{I_{\text{up}}}{2\pi H}; \quad \theta = \frac{T - T_{ci}}{T_{hi} - T_{ci}}$$

Their final forms were Eqs. (2)–(4):

$$\frac{\partial U}{\partial X} + \frac{\partial V}{\partial Y} = 0 \tag{2}$$

$$U\frac{\partial U}{\partial X} + V\frac{\partial U}{\partial Y} = -\frac{\partial P}{\partial X} + \frac{\mu_{nf}}{\mu}\frac{\rho_w}{\rho_{nf}}\frac{1}{\text{Re}}\left[\frac{\partial^2 U}{\partial X^2} + \frac{\partial^2 U}{\partial Y^2}\right]$$
$$+ \frac{\sigma_{nf}}{\sigma_w}\frac{\rho_w}{\rho_{nf}}\frac{\text{Ha}^2}{\text{Re}}\left[V\bar{B}_X\bar{B}_Y - U\bar{B}_Y^2\right] \tag{3a}$$

$$U\frac{\partial V}{\partial X} + V\frac{\partial V}{\partial Y} = -\frac{\partial P}{\partial Y} + \frac{\mu_{nf}}{\mu}\frac{\rho_w}{\rho_{nf}}\frac{1}{\text{Re}}\left[\frac{\partial^2 V}{\partial X^2} + \frac{\partial^2 V}{\partial Y^2}\right]$$
$$+ \frac{\sigma_{nf}}{\sigma_w}\frac{\rho_w}{\rho_{nf}}\frac{\text{Ha}^2}{\text{Re}}\left[U\bar{B}_X\bar{B}_Y - V\bar{B}_Y^2\right] \tag{3b}$$

$$U\frac{\partial \theta}{\partial X} + V\frac{\partial \theta}{\partial Y} = \frac{k_{nf}}{k_w}\frac{(\rho C_p)_w}{(\rho C_p)_{nf}}\frac{1}{\text{Re}\,\text{Pr}}\left[\frac{\partial^2 \theta}{\partial X^2} + \frac{\partial^2 \theta}{\partial Y^2}\right]$$
$$+ \frac{\sigma_{nf}}{\sigma_w}\frac{(\rho C_p)_w}{(\rho C_p)_{nf}}\text{Ec}\frac{\text{Ha}^2}{\text{Re}}\left[U\bar{B}_Y - V\bar{B}_Y^2\right]^2 \tag{4}$$

Fig. 1. Physical domain.

The expressions of the dimensional groupings appearing in the equations were:

$$Re = \frac{\rho_w U_{ci} H}{\mu}; \quad Ha = \left(\frac{\sigma_w B_0^2 H^2}{\mu}\right)^{1/2}; \quad Pr = \frac{\mu C_{pw}}{k_w};$$

$$Ec = \frac{U_{ci}^2}{C_{pw}(T_{hi} - T_{ci})}; \quad R_I = \frac{I_l}{I_{up}}$$

where Re, Ha, Pr, Ec, and R_I are the Reynolds number, the Hartmann number, the Prandtl number, the Eckert number, and the intensity ratio.

2.3. Boundary conditions

The following boundary conditions were associated with the previous governing equations:

Inlet: $X = 0, \; 0 < Y < 1/2 : U = 1; V = 0; \theta = 1$

$$1/2 < Y < 1 : U = 1; V = 0; \theta = 0 \tag{5}$$

Outlet: $X = L \quad \dfrac{\partial U}{\partial X} = 0; V = 0; \dfrac{\partial \theta}{\partial X} = 0 \tag{6}$

Lower plate: $Y = 0 \quad U = 0; V = 0; \dfrac{\partial \theta}{\partial Y} = 0 \tag{7}$

Upper plate: $Y = 1 \quad U = 0; V = 0; \dfrac{\partial \theta}{\partial Y} = 0 \tag{8}$

Wavy plate:

$$Y = \frac{1}{2} + A\sin(2\pi n X / L) \quad U = 0; \quad V = 0; \quad \left.\frac{\partial \theta}{\partial X}\right|_h = \left.\frac{\partial \theta}{\partial X}\right|_c; \quad \left.\frac{\partial \theta}{\partial Y}\right|_h = \left.\frac{\partial \theta}{\partial Y}\right|_c \tag{9}$$

2.4. Heat exchanger effectiveness

The heat exchanger effectiveness was defined as Eq. (10):

$$\varepsilon = \frac{C_h(\theta_{hi} - \theta_{ho})}{C_{min}(\theta_{hi} - \theta_{ci})} = \frac{C_c(\theta_{co} - \theta_{ci})}{C_{min}(\theta_{hi} - \theta_{ci})}; \quad C_{h,c} = \left[\left(\dot{m} C_p\right)_{nf}\right]_{h,c};$$

$$C_{min} = min\left[C_h, C_c\right] \tag{10}$$

The impact of the magnetic field on the heat exchanger effectiveness was evaluated by the ratio η_{Ha} calculated as follows:

$$\eta_{Ha} = \frac{\varepsilon(Ha \neq 0)}{\varepsilon(Ha = 0)} \tag{11}$$

To analyze the effect of the intensity ratio on the heat exchanger effectiveness, the ratio η_{RI} was introduced Eq. (12):

$$\eta_{R_I} = \frac{\varepsilon(R_I \neq 1)}{\varepsilon(R_I = 1)} \tag{12}$$

3. Numerical procedure

The governing equations with the associated boundary conditions were solved using the finite volume approach [13], whose basic idea was to convert these equations into algebraic ones to be solved numerically. The velocity components and pressure were coupled by a staggered grid, and the terms of diffusion and convection were discretized using the power-law scheme. The line-by-line approach, which connects the iterative Gauss-Seidel and the direct TDMA (Tridiagonal Matrix Algorithm) methods, was utilized as the solution procedure. After thorough testing, it was found that the numerical solution became slightly affected by the mesh size from a grid system of 500 nodes in the axial direction and 150 nodes in the transverse one. The relative error between two subsequent iterations must be smaller than 10^{-6} for each variable to meet the convergence condition.

4. Results and discussion

The physical phenomenon assessed was affected by numerous control parameters; thus, it was required to fix some and vary others to emphasize those most pertinent to the current investigation. To achieve this, the following parameters were selected: a heat exchanger's length $L = 20$, the base fluid water, the nanoparticles volume fraction $\phi = 5\%$, the same mass flow rates $\dot{m}_c = \dot{m}_f$ and the undulations number $n = 10$. On the other hand, the following parameters were varied: the Hartmann number Ha, the intensity ratio R_I, and the dimensionless undulation amplitude $A = a'/H$.

Fig. 2 illustrates the streamlines and isotherms evolutions in the heat exchanger for different values of Ha. The flow was disrupted due to the undulation of the inner wall and the presence of the magnetic field. These disturbances were more and more significant at increasing Ha with the appearance of stagnation zones near the magnetic sources at high Hartmann numbers. The effect of the Lorentz force was to slow the flow of the nanofluid, which would impact the thermal field structure. Indeed, by increasing the value Ha, the fluid path in the heat exchanger would be longer, and therefore, the heat exchange between the hot and cold fluids would be greater.

The impact of the undulation amplitude on the streamlines and the temperature field is shown in Fig. 3. In the case of a flat plate ($A = 0$), the applied magnetic field generated a perturbation of the nanofluid flow located in the action zone of the sources. The undulations caused more disturbances that spread over the entire length of the heat exchanger, with their magnitude increasing with a rise in A. Thermally, increasing the amplitude promoted the exchange between the two fluids, one of which became less hot and the other less cold.

As indicated in Fig. 4, the heat exchanger's effectiveness was influenced by the presence of the magnetic field and the internal wall's undulation. The increase of the Lorentz force slowed the nanofluid flow in the two compartments, whereas the rise in the undulation amplitude lengthened the path of the two fluids in the heat exchanger. As a result, more convective heat exchange has been accomplished, and consequently, ε increased with Ha and A. Indeed, the heat
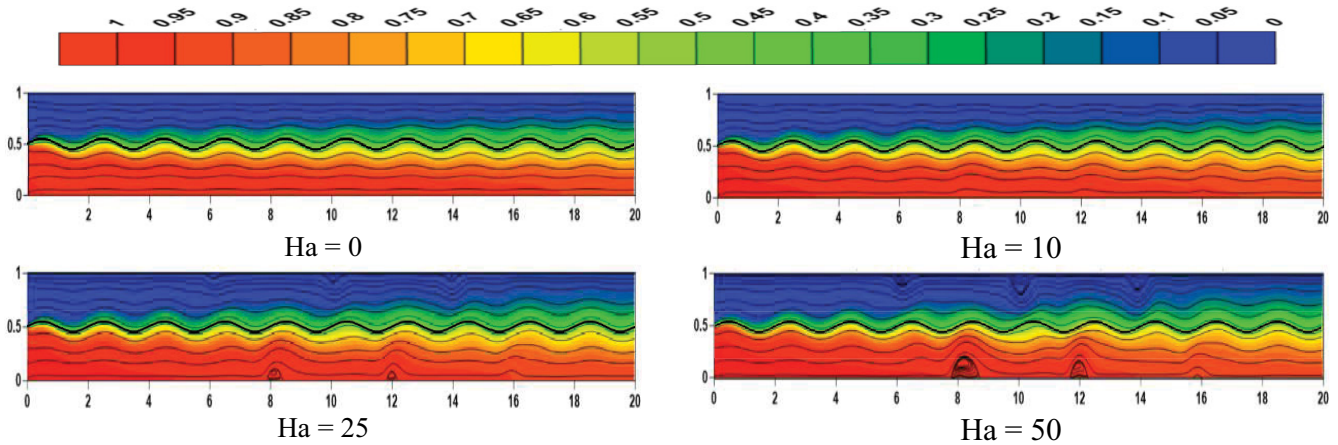
Fig. 2. Isocontours maps for various values of the Hartmann number, $R_I = 1$ and $A = 0.05$.
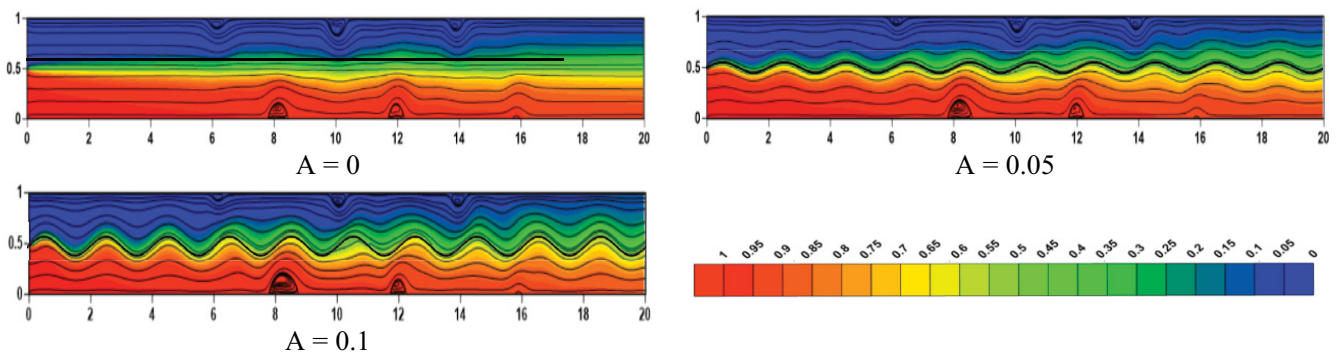
Fig. 3. Streamlines and isotherms for different values of the undulation amplitude, Ha = 40 and $R_I = 1$.
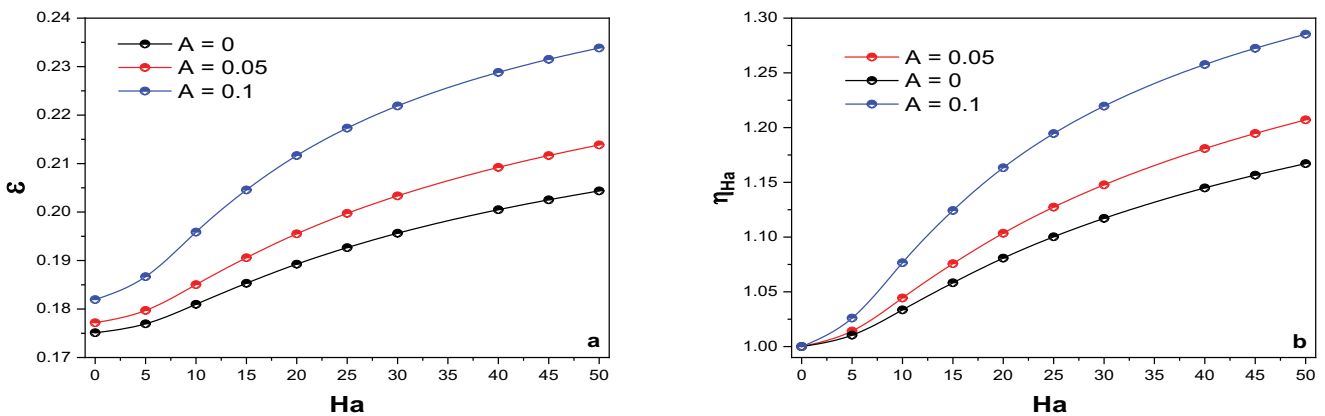
Fig. 4. Evolution of (ε, η_{Ha}) with the Hartmann number for different values of A and $R_I = 1$.

transfer enhancement between the hot and cold liquids led to an increase in the mean cold fluid's temperature and a reduction in that of the hot nanofluid, thus improving ε.

To examine the impact of a non-uniform magnetic field on the heat exchanger performance, ε was normalized by its corresponding value obtained by deactivating the sources (Ha = 0). Fig. 4b shows that applying a magnetic field was beneficial since the ratio η_{Ha} was always greater than unity.

The improvement rates increased with Ha and A, with maximum values varying between 16% and 28% when A went from 0 to 0.1.

With regards to the effect of the intensity ratio, it appeared from Fig. 5 that for R_I values less than the unity, the disturbances were more apparent in the cold nanofluid compartment. As the intensity ratio increased, the perturbations in the hot nanofluid compartment became significant and even

extend to the channel where the cold nanofluid circulated. Increasing R_I affected the lower compartment's flow and heat transfer characteristics, like increasing Ha while keeping $R_I = 1$. At high values of this ratio ($R_I = 5$), large stagnation zones appeared near the lower sources due to the slowing effect of the Lorentz force in this heat exchanger region. Another recirculation zone developed in the upper compartment, more precisely in the region of maximum interaction between the upper and lower sources. From a thermal point of view, increasing R_I, and thus raising the nanofluid disturbances, enhanced the heat transfer between the hot and the cold fluids, particularly in the interaction zone of magnetic sources.

Fig. 6a depicts the curves showing the heat exchanger effectiveness variation with the intensity ratio. An increase of ε was observed with the intensity ratio. In fact, by increasing the R_I value, more flow disruptions were experienced in the lower compartment and even extended to the upper one, as shown in Fig. 5. Consequently, the amount of heat exchanged between the two nanofluids improved, leading to increased heat exchanger effectiveness. This augmentation was more apparent for R_I values greater than unity and at high undulation amplitude. As long as the intensity ratio was lower than unity, the variation of R_I seemed to be thermally non-beneficial and would only become so for $R_I > 1$. In this case, the improvement rates increased with R_I and A. Their maximum values varied between 7.5% and 17% when A went from 0 to 0.1.

5. Conclusions

The main objective of this numerical study was to analyze the effects of a magnetic field on the performance of a plate heat exchanger with a wavy inner wall. The most relevant findings were:

- The flow disturbances in the two compartments of the heat exchanger became more significant as the Hartmann number, intensity ratio, and undulation amplitude are high.
- The heat exchanger effectiveness was improved by increasing Ha, A, and R_I.
- Applying a non-uniform magnetic field was beneficial since η_{Ha} was always greater than unity whatever the control parameters values. The highest value of η_{Ha} was around 28% obtained for the combination Ha = 50 and $A = 0.1$ for $R_I = 1$.
- The non-uniformity of the electric current crossing the magnetic sources was only efficient when the intensity ratio was greater than unity. In this case, $\eta_{RI} > 1$ with its highest value around 17% obtained for the combination $R_I = 5$ and $A = 0.1$ for Ha = 25.

As an extension of this work, we suggest using different types of corrugations, examining the impact of the nanoparticles' type and volume fraction, analyzing the number and the arrangement of the magnetic sources to achieve the best
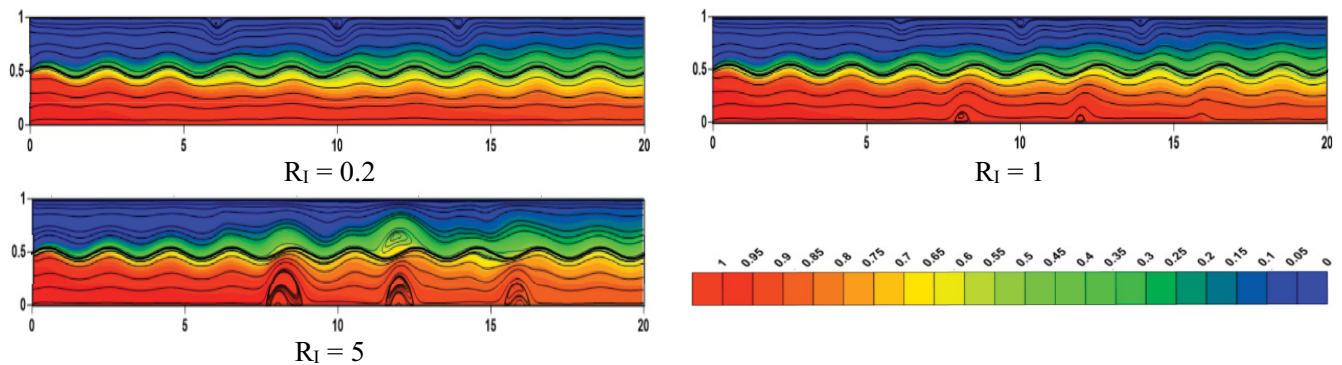
Fig. 5. Streamlines and isotherms for different values of the intensity ratio, Ha = 25 and $A = 0.05$.
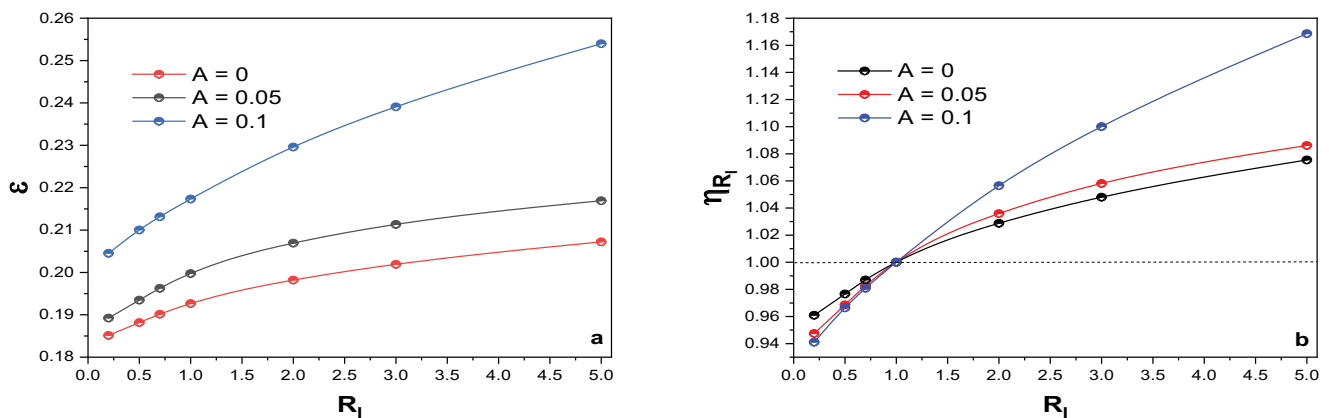
Fig. 6. Evolution of (ε, η_{R_I}) with the intensity ratio for different values of A and Ha = 25.

performance factors, and finally performing measurements on a real experimental device.

Symbols

C_p	—	Specific heat at constant pressure, $J \cdot kg^{-1} \cdot K^{-1}$
k	—	Thermal conductivity, $W \cdot m^{-1} \cdot K^{-1}$
p	—	Pression, Pa
T	—	Temperature, K
u, v	—	Velocity components, $m \cdot s^{-1}$
x, y	—	Axial and transverse coordinates, m

Greek

θ	—	Dimensionless temperature
μ	—	Dynamic viscosity, $kg \cdot m^{-1} \cdot s^{-1}$
μ_0	—	Magnetic permeability of vacuum, $T \cdot m \cdot A^{-1}$
ε	—	Heat exchanger effectiveness
ρ	—	Density, $kg \cdot m^{-3}$
σ	—	Electrical conductivity, $\Omega^{-1} \cdot m^{-1}$

Subscripts

c	—	Cold
h	—	Hot
i	—	Inlet
l	—	Lower
nf	—	Nanofluid
o	—	Outlet
up	—	Upper
w	—	Base fluid (water)

References

[1] D. Zheng, J. Wang, Z. Chen, J. Baleta, B. Sundén, Performance analysis of a plate heat exchanger using various nanofluids, Int. J. Heat Mass Transfer, 156 (2020) 119993, doi: 10.1016/j.ijheatmasstransfer.2020.119993.

[2] M. Karuppasamy, R. Saravanan, M. Chandrasekaran, V. Muthuraman, Numerical exploration of heat transfer in a heat exchanger tube with cone shape inserts and Al_2O_3 and CuO nanofluids, Mater. Today:. Proc., 21 (2020) 940–947.

[3] M. Biheraei, M. Naseri, A. Monavari, Thermal-hydraulic performance of a nanofluid in a shell-and-tube heat exchanger equipped with new trapezoidal inclined baffles: nanoparticle shape effect, Powder Technol., 395 (2022) 348–359.

[4] A.M. Alklaibi, L.S. Sundar, K.V.V.C. Mouli, Experimental investigation on the performance of hybrid Fe_3O_4 coated MWCNT/Water nanofluid as a coolant of a plate heat exchanger, Int. J. Therm. Sci., 171 (2022) 107249, doi: 10.1016/j.ijthermalsci.2021.107249.

[5] M. Biharaei, M. Hangi, Investigating the efficacy of magnetic nanofluid as a coolant in double-pipe heat exchanger in the presence of magnetic field, Energy Convers. Manage., 76 (2013) 1125–1133.

[6] S.V. Mousavi, M. Sheikholeslami, M.G. Bandpy, M.B. Gerdroodbary, The influence of magnetic field on heat transfer of magnetic nanofluid in a sinusoidal double pipe heat exchanger, Chem. Eng. Res. Des., 113 (2016) 112–124.

[7] A. Shakiba, K. Vahedi, Numerical analysis of magnetic field effects on hydro-thermal behavior of a magnetic nanofluid in a double pipe heat exchanger, J. Magn. Magn. Mater., 402 (2016) 131–142.

[8] P. Naphon, S. Wiriyasart, Pulsating flow and magnetic field effects on the convective heat transfer of TiO_2-water nanofluids in helically corrugated tube, Int. J. Heat Mass Transfer, 125 (2018) 1054–1060.

[9] S. Mei, C. Qi, T. Luo, X. Zhai, Y. Yan, Effects of magnetic field on thermo-hydraulic performance of Fe_3O_4-water nanofluids in a corrugated tube, Int. J. Heat Mass Transfer, 128 (2019) 24–45.

[10] G. Wang, C. Qi, M. Liu, C. Li, Y. Yan, L. Liang, Effect of corrugation pitch on thermo-hydraulic performance of nanofluids in corrugated tubes of heat exchanger system based on exergy efficiency, Energy Convers. Manage., 186 (2019) 51–65.

[11] F. Fan, C. Qi, J. Tang, Q. Liu, X. Wang, Y. Yan, A novel thermal efficiency analysis on the thermo-hydraulic performance of nanofluids in an improved heat exchange system under adjustable magnetic field, Appl. Therm. Eng., 179 (2020) 115688, doi: 10.1016/j.applthermaleng.2020.115688.

[12] Y. Cao, H. Ayed, F. Jarad, H. Togun, H. Alias, A. Issakhov, M. Dahari, M. Wae-hayee, M.H. El Ouni, MHD natural convection nanofluid flow in a heat exchanger: effects of Brownian motion and thermophoresis for nanoparticles distribution, Case Stud. Therm. Eng., 28 (2021) 101394, doi: 10.1016/j.csite.2021.101394.

[13] S.V. Patankar, Numerical Heat Transfer and Fluid Flow, McGraw-Hill, New York, 1980.